Definition of out-of-plane fragility curves for masonry infills subject to combined in-plane and out-of-plane damage

Definition of out-of-plane fragility curves for masonry infills subject to combined in-plane and out-of-plane damage

F. Di Trapani, M. Malavisi
Politecnico di Torino, Department of Structural, Building and Geotechnical Engineering, Turin, Italy

P.B. Shing
University of California at San Diego, Department of Structural and Material Engineering, La Jolla, CA

L. Cavaleri
University of Palermo, Dipartimento di Ingegneria, Palermo, Italy

ABSTRACT: The paper presents the outcomes of a probabilistic assessment framework aimed at defining out-of-plane fragility curves of unreinforced masonry infills walls which have been subjected (or not) prior in-plane damage. A recently developed in-plane (IP)/out-of-plane (OOP) four-strut macro-element model is used to model masonry infills within frames. Out-of-plane incremental dynamic analyses are performed, for a reference infilled frame, based on a suite of 26 ground motion record selection. Peak ground acceleration (PGA) and OOP relative displacement of the midspan node of the infill, are used as intensity measure and damage measure. The outcomes show fragility curves representing the probability of exceeding out-of-plane collapse at a given earthquake intensity as a function of a different combination of geometrical and mechanical parameters, in-plane damage level and supporting conditions. Results are finally summarized by curves relating in-plane interstorey drifts and out-of-plane average collapse PGA.

1 INTRODUCTION

In the last years, the out-of-plane (OOP) earthquake response of masonry infills and its mutual dependence with the in-plane (IP) damage level has received special interest by researchers (e.g. Mazza et al. 2019, Di Trapani et al. 2020a). New experimental and numerical investigations (e.g. Furtado et al. 2016, Ricci et al. 2018, De Risi et al. 2019, Cavaleri et al. 2019) have been carried out and, at the same time, new simplified models able to predict both in-plane and out-of-plane responses have been developed following different mechanical approaches (Mosalam and Günay 2014, Furtado et al. 2015, Di Trapani et al. 2018a). The response of masonry infilled reinforced concrete (RC) frame buildings subject to ground motions inducing in-plane and out-of-plane actions is not of easy generalization as this depends on several aspects as the geometrical configuration of the frame, the position of the infills along the height, the reciprocal earthquake intensity along the two orthogonal directions. Some recent studies referred to the analysis entire buildings (Ricci et al. 2019, Longo et al. 2019) have confirmed this. In fact, infills located at the highest floor are subjected to major accelerations but at the same time lower in-plane damage. Conversely, infills at the lowest floors undergo reduced accelerations demand but suffer large in-plane drift demand that waken their out-of-plane capacity. Considering these premises, a prediction of the most critical conditions for the infill walls in a frame structure cannot be carried in a simple way in case of combined IP-OOP actions.

In this paper the issue is faced using a probabilistic assessment framework aimed at evaluating out-of-plane fragility curves of infill walls which have been subjected (or not) prior in-plane damage. The fiber-section macro-element model by Di Trapani et al. (2018a) is used to model the infill wall. Fragility curves are obtained performing out-of-plane incremental dynamic analyses (IDA) based on a suite of 26 ground motion records. IDA curves, and the associated fragilities are obtained by varying the slenderness ratio, the in-plane drift level, and the frame stiffness with respect to the out-of-plane stiffness of the infill.

2 DESCRIPTION OF THE MACROELEMENT MODEL AND DETERMINATION OF THE EQUIVALENT OOP MASS

2.1 *Definition of the microelement model*

The macro-element model by Di Trapani et al. (2018a) provides the replacement of the infill panel with 4 pinned struts, each one divided into two elements. The overall scheme is illustrated in Fig. 1a. Each strut is defined using distributed plasticity fiber-section beam-column elements available in OpenSees.

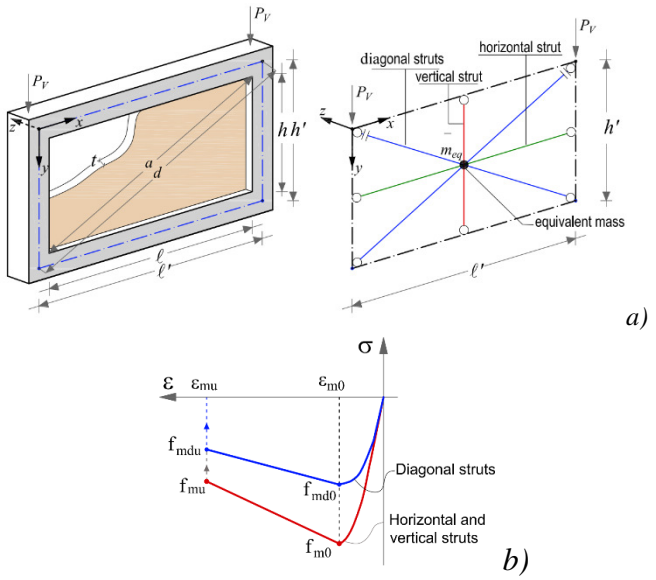

Figure 1. Definition of the 4-strut macro-model: a) Geometric definition; b) Stress-strain models for the struts.

In this way, internal cross-section forces of these elements are related to the corresponding deformations (axial deformation and curvature), hence, after the elastic stage axial load is coupled with bending moment and the arching mechanism is then naturally accounted. The diagonal, horizontal and vertical struts have typical concrete-type stress-strain laws, modelled with the OpenSees Concrete02 material (Fig. 1b). Moreover, in order to explicitly consider the effects of strength degradation, the Concrete02 material model is combined with the MinMax material so that, once the ultimate strain is achieved at a generic fiber, the corresponding stress drops to zero. The diagonal struts are constrained with pins at the ends. They provide the whole in-plane response of the infill as well as the main OOP contribution. The horizontal and vertical struts provide a complementary OOP contribution to strength, reproducing the 2-way bending effect of the panel. The 4 struts do not share the mid-span node but are constrained to move together along the z direction. In this way each strut can provide its strength contribution to the OOP response. Geometrical and mechanical identification of the struts is performed starting from the diagonals, whose force-displacement behaviour can be assigned by adopting any method. Once that the force-displacement law is determined, this can be easily converted into an equivalent concrete-type stress-strain relationship and assigned to the cross-section fibers. To perform this step, the reference cross-section can be simply obtained by fixing the width (w_d) as 1/3 of the internal diagonal length (a) and the thickness as the actual thickness (t) of the infill. A direct definition of the stress-strain relationship and width of the diagonal cross-sections can also carried out by using the approach by Di Trapani et al. (2018b). When defining the stress-strain relationship of the diagonal struts it can be easily found that the peak strength f_{md0} is lower than the actual compressive strength of masonry (f_{m0}). This is due to the fact that f_{md0} expresses a fictitious resistance which summarized the complex response of the infill subject to lateral forces. On the other hand, the out-of-plane strength is proportional to the actual compressive strength of the masonry (f_{m0}). In order to compensate the drawback, the cross-section thickness of the strut is increased by the ratio f_{m0}/f_{md0}, so that:

$$\tilde{t} = \frac{f_{m0}}{f_{md0}} t \tag{1}$$

while, in order to maintain unaltered the cross-section area, the width is reduced as:

$$\tilde{w}_d = \frac{t}{\tilde{t}} w_d \tag{2}$$

The residual OOP strength is provided by the horizontal and vertical struts. The latter are defined using the actual thickness t of the infill and the actual strength f_{m0}, while the widths are obtained as the difference between the height and the length of the panel and the horizontal and vertical projections of the diagonal initial width w_d on the infill perimeter. The widths of the horizontal strut (w_h) and vertical strut (w_v) are therefore evaluated as follows:

$$w_h = h - \frac{w_d}{\cos\theta}; \quad w_v = \ell - \frac{w_d}{\sin\theta} \tag{3}$$

where θ is the inclination of the strut with respect to the horizontal direction.

2.2 *Definition of the equivalent mass*

In order to perform dynamic simulations, the model needs the definition of an equivalent mass to apply at the midspan node of the struts. The mass (m_{eq}) of the so defined single degree of freedom (SDOF) system is of course a percentage of the total mass of the infill. In order to identify this percentage, an experimental/numerical identification procedure has performed using the results of the experimental tests by Angel (1994). The same tests which were also used for the validation of the aforementioned model. The tests regarded reinforced concrete infilled frame specimens subject to in-plane cycles and then pushed out-of-plane using an airbag. The identification procedure consists of the following steps: *a*) determination of the experimental out-of-plane stiffness K_{exp} from the experimental force-displacement diagrams; *b*) identification of the out-of-plane period of the infill ($T_{i,FEM}$) by defining an elastic finite element model of a plate pinned at the sides (Fig. 2), verifying that the stiffness of the plate (K_{FEM}) was the same as the experimental stiffness; *c*) determination of the equivalent mass of the SDOF system as:

$$m_{eq} = \frac{T_{i,FEM}^2}{4\pi^2} K_{exp} \tag{4}$$

In the procedure it is assumed that the out-of-plane stiffness provided by the macro-model is the same as that the experimental stiffness. This was proved by the validation tests presented in Di Trapani et al. (2018a) for the same specimens. It should be also observed that that since the specimen were subjected to moderate cycles before being tests out-of-plane, their experimental stiffness was lower with respect to that estimated by the elastic FE model of the plate. Therefore, the matching between K_{FEM} and K_{exp} was obtained by modifying the elastic modulus of the infill (E_m) into a lower one (E_m^*). This manipulation has no influence on the equivalent mass value found by Eq. (4), with respect to an undamaged case, since the reduction of K_{FEM} due to the reduction of E_m in the FE model, is compensated by the elongation of the period. Geometric dimensions and masses of the infills of specimens by Angel (1994) are reported in Table 1. Mechanical properties of the infills are reported in Table 2 together with the obtained experimental stiffness values, periods and equivalent masses. It is noteworthy observing that independently on the different geometric and mechanical combinations of the specimens the percentage equivalent mass resulted 55% of the total mass on average. This allows concluding that the macro-element model can be adapted to perform dynamic simulations by assigning a 55% equivalent mass at the central node.

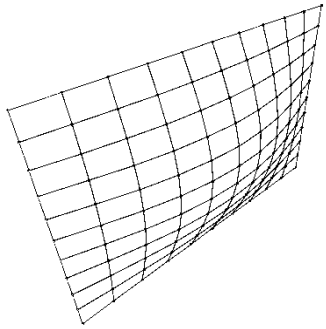

Figure 2. First modal shape of the FE model of the infill.

Table 1. Geometric dimensions and masses of specimens by Angel (1994).

Spec.	ℓ	ℓ'	h	h'	t	h/t	γ	mass
	(mm)	(mm)	(mm)	(mm)	(mm)	(-)	(kN/m^3)	(kg)
2	2440	2740	1630	1930	47.6	34.2	19	359.7
3	2440	2740	1630	1930	47.6	34.2	19	359.7
4	2440	2740	1630	1930	92.0	17.7	19	695.2
5	2440	2740	1630	1930	143.0	11.4	19	1080.6
6	2440	2740	1630	1930	98.4	16.6	19	743.6

Table 2. Mechanical properties and identification parameters of specimens tested by Angel (1994).

Spec.	E_m	G_m	E_m^*	f_{m0}	K_{exp}	$T_{i,FEM}$	m_{eq}	$m_{eq\%}$
	(MPa)	(MPa)	(MPa)	(MPa)	(N/mm)	(s)	(kg)	(%)
2	8040	8040	1900	10.85	1052.6	0.083	184.5	51.3
3	5208	5208	1736	10.13	1300	0.078	202.3	56.2
4	12429	12429	5000	22.90	20000	0.027	364.2	52.4
5	11616	11616	9000	22.82	148000	0.012	582.6	53.9
6	2136	2136	650	4.60	3500	0.070	429.0	57.7

3 ANALYSIS FRAMEWORK

3.1 *Analysis program*

The investigation is first addressed to the derivation of out-of-plane fragility curves of a one-storey infilled frame as a function of different boundary conditions, that is the slenderness ratio and strength of the specimen, the extent of the previous in-plane damage, the out-of-plane vibration period of the infill with respect to that of the supporting frame structure. Two reference specimens among those tested by Angel (1994) have been selected to perform fragility assessment, namely Specimen 2 and Specimen 6. These specimens have different slenderness ratios and masonry strength as it can be observed from Tables 1 and 2. The OOP resistance of a masonry infills (F_r) can be estimated through the EC6 expression as:

$$F_r = f_{m0}\left(\frac{t}{h'}\right)^2 \ell h \tag{5}$$

From Eq.(5) one can determine the OOP resisting pressure (f_r) as:

$$f_r = \frac{F_r}{\ell h} \tag{6}$$

This parameter combines both strength and slenderness ratio, and so it can be used to identify a class of infilled frames. For specimens 2 and 6 f_r was 6.6 MPa and 11.95 MPa respectively.

In order to simulate the influence of the supporting frame, the reference infilled frame is modelled as in Fig. 3, where besides the equivalent mass at the midspan node, the model has 4 mass-spring (m_f ,k_f) systems at the corner nodes. The whole system has therefore two degrees of freedom, one related to the frame, the other related to the infill. The vibration period associated with the frame considered alone can be obtained as:

$$T_f = 2\pi\sqrt{\frac{M_f}{K_f}} \tag{7}$$

in which $M_f=4m_f$ is the total mass of the frame $K_f=4k_f$ is the total stiffness of the parallel springs. The vibration periods associated with the infills have been obtained as described in the previous section ($T_i = T_{i,FEM}$). The springs have elastic behaviour and are modelled in OpenSees using zero-length elements. For the two specimens under investigation, the response of the system is analyzed considering five different supporting conditions, namely rigid support ($K_f=\infty$), $T_f=T_i$, $T_f=3T_i$, $T_f=5T_i$, $T_f=7T_i$. Given that the period of the infills is fixed, and attributing a conventional mass (m_f) of 2000 kg to the nodes of the frames, the stiffness of the frame producing the aforementioned period ratios can be obtained as:

$$K_f = 4\pi^2 \frac{M_f}{T_f^2} \tag{8}$$

and then:

$$k_f = 4\pi^2 \frac{m_f}{T_f^2} \tag{9}$$

The effect of prior in-plane damage is also investigated considering 4 cases, namely: a) no in-plane damage; b) IDR=0.5%; c) IDR=1.5%; d) IDR=2.5%. The IDR (interstorey drift) is assumed as measure of the in-plane damage. The analyses are carried out in OpenSees through two-steps. First a cyclic static analysis consisting of three cycles having amplitude as the fixed IDR is performed. Subsequently the IDA sequence is started. A summary of the analyses is reported in Table 3. Details about periods, and stiffness of the different systems obtained for Specs. 2 and 6 are listed in Tables 4 and 5.

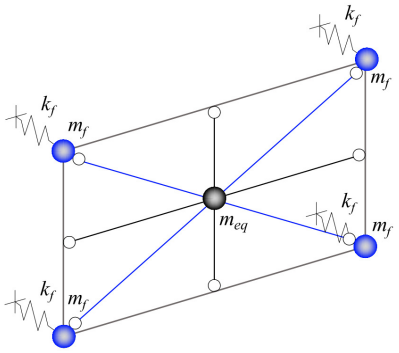

Figure 3. Reference scheme for the infilled frame model.

Table 3. Summary of the test conditions.

Support conditions	Specimen 2 IDR (%)	Specimen 6 IDR (%)
T_f=0 (Rigid frame)	0 / 0.5 / 1.5 / 2.5	0 / 0.5 / 1.5 / 2.5
$T_f=T_i$	0 / 0.5 / 1.5 / 2.5	0 / 0.5 / 1.5 / 2.5
$T_f=3T_i$	0 / 0.5 / 1.5 / 2.5	0 / 0.5 / 1.5 / 2.5
$T_f=5T_i$	0 / 0.5 / 1.5 / 2.5	0 / 0.5 / 1.5 / 2.5
$T_f=7T_i$	0 / 0.5 / 1.5 / 2.5	0 / 0.5 / 1.5 / 2.5

Table 4. Period, mass and stiffness values of the systems obtained by Spec. 2

T_f/T_i (-)	T_i (s)	T_f (s)	M_f (kg)	K_f (kN/m)	k_f (kN/m)
0	0.083	0	8000	∞	∞
1	0.083	0.083	8000	3801.3	950.3
3	0.083	0.249	8000	1267.1	316.8
5	0.083	0.415	8000	760.3	190.1
7	0.083	0.581	8000	543.0	135.8

3.2 *Definition of IDA curves*

Incremental Dynamic Analysis (IDA) (Vamvatsikos and Cornell, 2002) has been used many times in recent years for the assessment of seismic fragility of structures (Basone et al. 2017, Di Trapani & Malavisi 2019, Di Trapani et al. 2020b). In the current case IDA has been carried out using the peak ground acceleration (PGA) as intensity measure (IM) and the out-of-plane net displacement (Δ_{OOP}) as damage measure (DM). 26 ground motions records have been considered. The spectra of the selected ground motion are shown in Fig. 4. The choice of PGA as IM instead of the usual spectral acceleration at of the first vibration period is due to the fact that, as explained in the previous section, different combinations of periods are considered. The choice of PGA allows using the same ground motion scaling to analyse the different combinations of periods. In detail the ground motions are first scaled so that their respective spectra have the same PGA. The subsequent scaling during IDA uniformly increases / decreases the amplitude. For each ground motion IDA are stopped in correspondence of the achievement of dynamic instability (which represents the OOP failure of the infill). After this point, a constant flatline is conventionally represented.

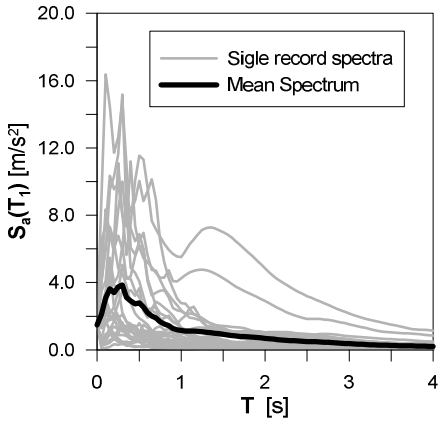

Figure 4. Ground motion selection spectra and average spectrum.

3.3 *Definition of fragility curves*

Fragility curves express the probability of exceeding a specified limit state as a function of the specified IM (PGA). Fragility curves can be represented using a lognormal cumulative distribution function as:

$$P[C \le D \mid IM = x] = \Phi\left(\frac{ln(x) - \mu_{ln_x}}{\sigma_{ln_x}}\right) \tag{10}$$

where $P[C \le D|IM=x]$ is the probability that a ground motion with IM=x will cause the achievement of a limit state, Φ is the standard cumulative distribution function, $ln(x)$ is the natural logarithm of the variable x representing the intensity measure (PGA) and μ_{lnX} and σ_{lnX} are the mean and the standard deviation of the natural logarithms of the distribution of x, respectively. Fragility curves are derived considering the collapse limit state, which is attained when the dynamic instability occurs during IDA or when the midspan relative displacement of the infill (Δ_{OOP}) is the same as the thickness of the infill. In this latter case, in fact, it is supposed that the arching action vanishes, and the equilibrium is no longer achieva-

ble. Cumulative discrete distribution functions are also overlapped to the analytically obtained fragility curves to verify the adequacy of the distribution model.

4 RESULTS FOR THE ONE-STOREY INFILLED FRAME

4.1 *IDA and fragility curves*

IDA curves are illustrated in Fig. 5-8 for the one-storey infilled frame for different considered combinations of T_f/T_i ratios and in-plane interstorey drifts. For sake of space, IDA curves are only reported for specimen 2. The curves show a reduction of the average collapse PGA when increasing T_f/T_i up to 3. After the collapse PGA tends to increase again, denoting that T_f/T_i ratio has a relevant role, as it influences the accelerations experienced by the infill wall. On the other hand, it should be also observed that the presence of in-plane damage (measured by the in-plane IDR) tends to reduce the influence of T_f/T_i. In fact in presence of severe damage (IDR=1.5.%-2.5%) the collapse PGA is dramatically reduced. Under these conditions no substantial differences can be observed when by varying T_f/T_i ratio. Fragility curves of the one-storey infilled frame are shown in Fig. 9.

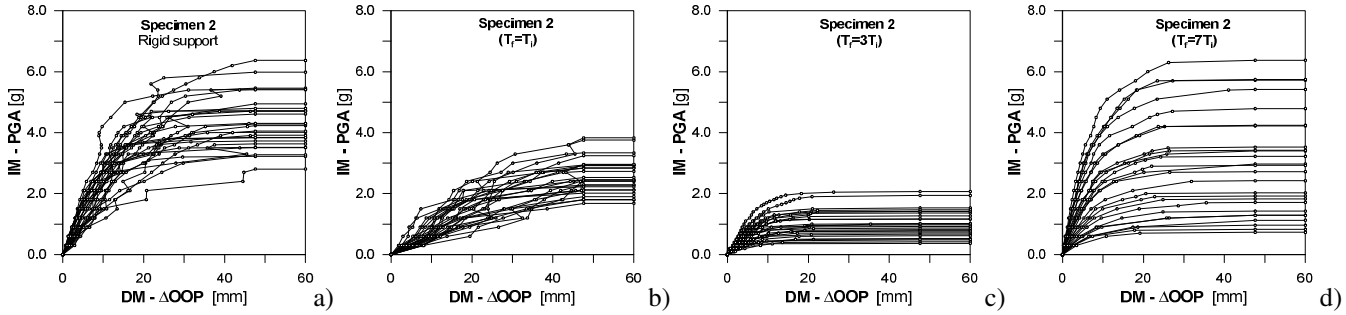

Figure 5. IDA curves of Specimen 2 without in-plane damage for: a) rigid support; b) $T_f=T_i$; b) $T_f=3T_i$; b) $T_f=7T_i$.

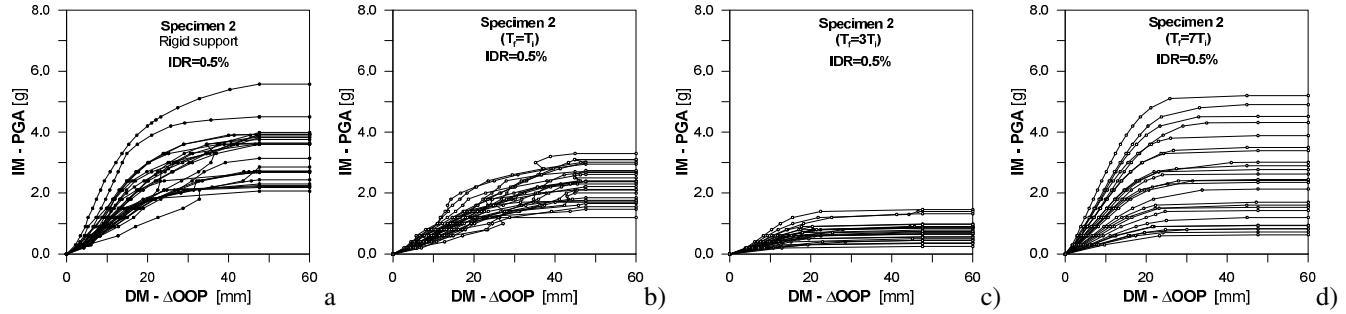

Figure 6. IDA curves of Specimen 2 with IDR=0.5% for: a) rigid support; b) $T_f=T_i$; b) $T_f=3T_i$; b) $T_f=7T_i$.

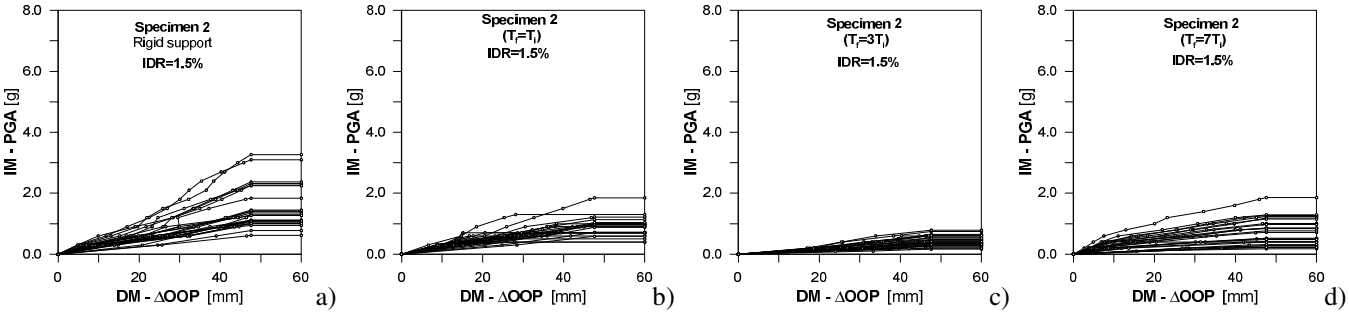

Figure 7. IDA curves of Specimen 2 with IDR=1.5% for: a) rigid support; b) $T_f=T_i$; b) $T_f=3T_i$; b) $T_f=7T_i$.

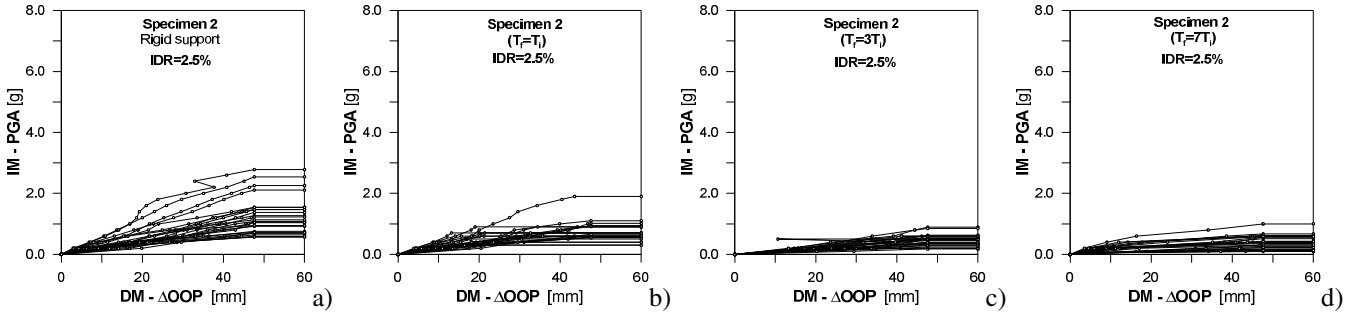

Figure 8. IDA curves of Specimen 2 with IDR=2.5% for: a) rigid support; b) $T_f=T_i$; b) $T_f=3T_i$; b) $T_f=7T_i$.

The latter reflect what already highlighted by IDA curves. For the case of no-IP damage and moderate IP damage (IDR=0.5%) (Figs. 9a-9b) fragility tends to increase when increasing T_f/T_i up to 3. After this point fragility tends to be reduced, although significantly larger dispersion of collapse IMs is observed. For the cases of high IP damage (Figs. 9b-9c) fragility curves result significantly shifted on the right denoting minor sensitivity to variation of T_f/T_i. In some cases, collapse PGA values may result very high, so that they can exceed a hypothetical collapse PGA for the frame. This is due to the elastic behaviour of the springs used to represent the response of the frame. In this cases OOP fragility curves lose significance since an overall collapse occurs before the OOP collapse of the infills.

In the next section the investigation is extended to the case of a multi-storey frame under the simplified assumption of linear distribution of floor accelerations

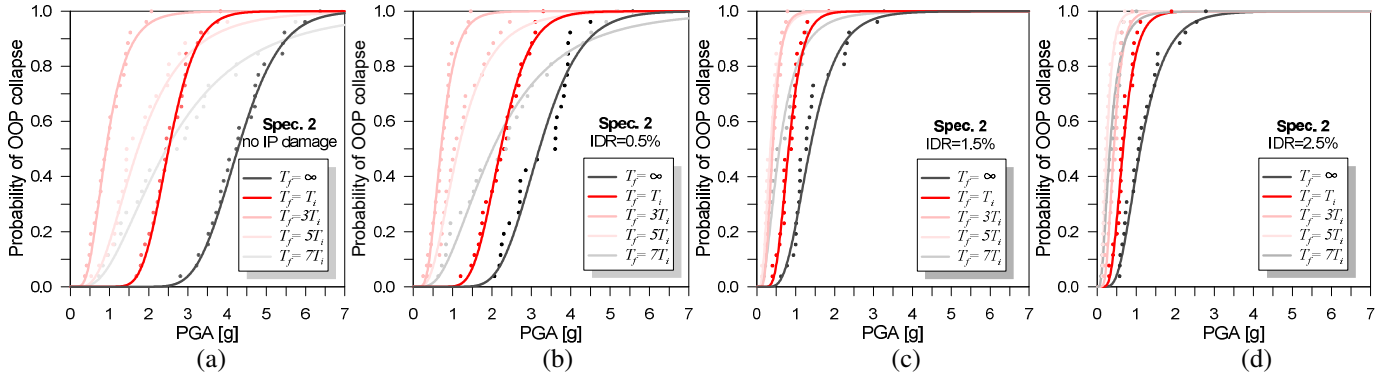

Figure 9. Fragility curves of specimen 2 for different T_f/T_i with: a) IDR=0 %; b) IDR=0.5 %; c) IDR=1.5 %; d) IDR=2.5 %.

5 EXTENSION TO MULTISTOREY INFILLED FRAMES

Results shown in the previous section are referred to the elementary one-storey infilled frame, which is supposed to be subjected to an acceleration history at the supports. In the case of a multi-storey frame, floor accelerations tend to grow when increasing the height, as also provided by EC6 through the expression:

$$S_a = PGA \cdot S \cdot \beta \tag{11}$$

where S is the soil factor, S_a the pseudo acceleration of an infill wall at the center of mass, positioned at the altitude (Z) from the ground in a building having total height (H) and β is a modulation factor defined as:

$$\beta = \frac{3(1+Z/H)}{1+(1-T_i/T_f)^2} - 0.5 \tag{12}$$

It is easy to demonstrate that according to Eq. (11) S_a increases with increasing the altitude of the infill with respect to the total height of the building, according to a linear relationship. Eq. (12) can be adapted to estimate floor acceleration demand variation for the analysed infilled frames. In this case, given that the effect of the variation of T_i/T_f ratio has been already taken into account in the previous analyses on the one-storey infilled frame, in Eq. (12) it can be set $T_i/T_f=0$. Finally, for consistency with the assumed scheme for the one-storey infilled frames, the values Z' and H' are used instead of Z and H, where Z' is the quote of the center of mass of the infill measured with respect to the center of mass of the first ground floor infill, and H' is the quote of the center of mass of the infill at the highest floor. Under these assumptions one obtains:

$$\beta^* = \frac{3(1+Z'/H')}{2} - 0.5 \tag{13}$$

It can be easily observed that if $Z'/H'=0$ (case of infill wall at the ground floor or one storey infilled frame), $\beta^*=1$ (no amplification is provided), while if $Z'/H'=1$ (case of infill wall at the top floor) one obtains the maximum amplification factor ($\beta^*=2.5$).

By defining $\overline{PGA}_{C,0}$ as the 50% probability PGA inducing the collapse of the one-storey infilled frame, it can be reasonably supposed that the average PGA inducing the collapse of an infill wall at the generic Z/H position ($\overline{PGA}_{C,(Z/H)}$) can be obtained by reducing $\overline{PGA}_{C,0}$ by β^*, therefore:

$$\overline{PGA}_{C,(Z/H)} = \frac{\overline{PGA}_{C,0}}{\beta^*} \tag{14}$$

The values of $\overline{PGA}_{C,0}$ extrapolated from the fragility curves of specimens 2 and 6 can be represented as in Figs. 10a and 11a as a function of T_f/T_i and IDR. This are coincident with $\overline{PGA}_{C,(Z/H)}$ at $Z'/H'=0$. Diagrams in Figs. 10b-c and 11b-c represent $\overline{PGA}_{C,(Z/H)}$ for $Z'/H'=0.5$ and $Z'/H'=1$. The latter are obtained from the first two diagrams by using Eq. (14). Diagrams in Figs. 10-11 show that infill at the higher stories undergo major spectral accelerations and therefore their collapse may occur with significantly reduced PGA levels. At the same time infills positioned at lower stories suffer major in-plane

damage. This means that their collapse may occur with lower PGA values, with respect to those inducing collapse of infills at the upper stories.

Diagrams in Figs. 10-11 can be also used as assessment tools by entering with the characteristics of the infilled frames and comparing the resulting average PGA with a design PGA level.

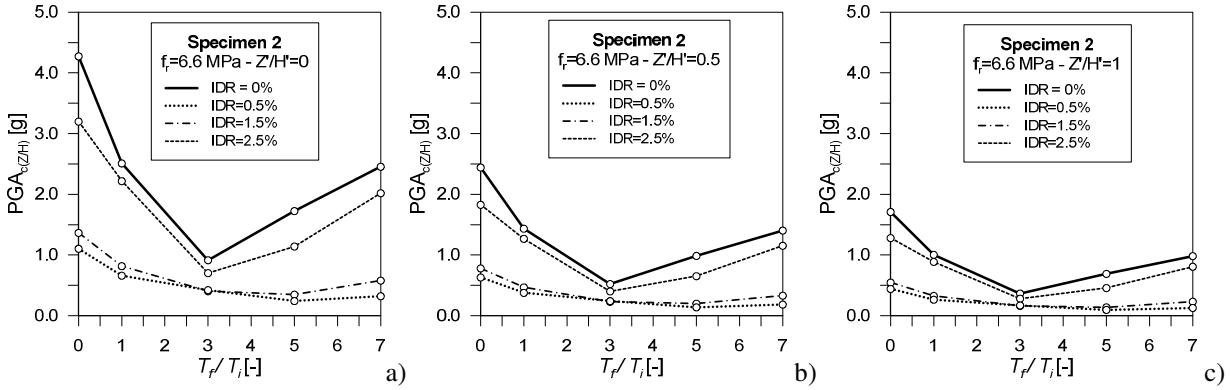

Figure 10. Average collapse PGA for Specimen 2 with: a) Z'/H'=0; b) Z'/H'=0.5; c) Z'/H'=1.0.

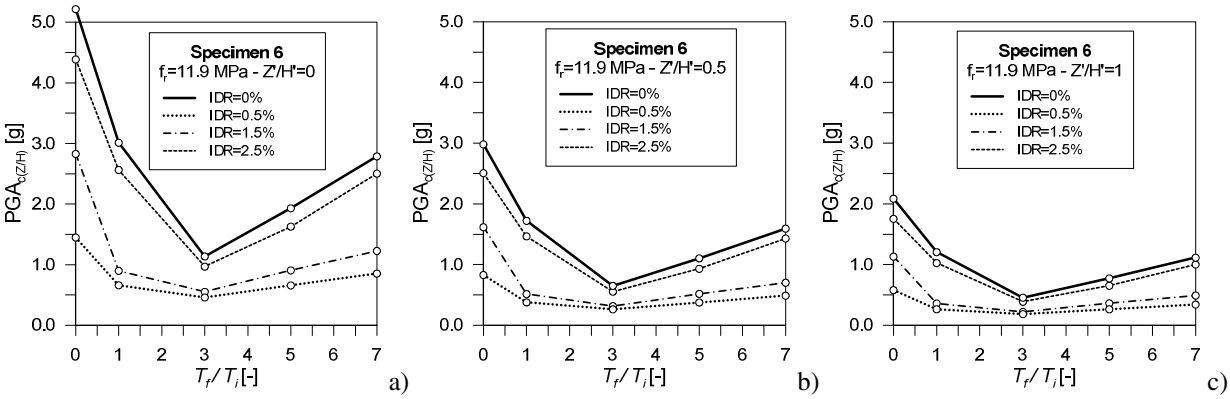

Figure 11. Average collapse PGA for Specimen 6 with: a) Z'/H'=0; b) Z'/H'=0.5; c) Z'/H'=1.0.

6 CONCLUSIONS

In the paper an existing infilled frame macro-element model (Di Trapani et al. 2018a) has been updated to perform dynamic simulations. The model consist of four fiber-section struts and is able to account for mutual in-plane and out-of-plane damage. Out-of-plane fragility curves for a reference one-storey infilled frames have been derived considering different prior IP damage levels and different ratios between frame and infill periods (T_f/T_i). Incremental dynamic analysis was used to derive fragility curves. Results have shown that for the cases of no-IP damage and moderate IP damage the average collapse PGA tend to increase when increasing T_f/T_i up to 3. After this point collapse PGA tends to be reduced. For the cases of severe IP damage, collapse PGA dramatically decreases denoting minor sensitivity to T_f/T_i. The analysis has been extended to multi storey infilled frames under the simplified assumption of linear distribution for floor accelerations. It has been shown that infills at the higher stories undergo major spectral acceleration and their collapse may be achieved in correspondence of reduced PGA values. However, infills positioned at lower stories undergo major in-plane damage potentially causing their anticipated collapse with respect to the upper stories infills. Therefore, the location of masonry infills subject to major OOP collapse risk in not predictable a priori as this depends on the combination between floor acceleration and in-plane drift at each storey.

Finally, average collapse PGA diagrams have been provided as a function of T_f/T_i , IDR and *Z'/H'*. The latter can be used as assessment tools by comparing the average PGA associated with a an infilled frame to design PGA level.

REFERENCES

Angel, R., 1994. Behavior of reinforced concrete frames with masonry infill walls. PhD thesis, *University Illinois at Urbana-Champaingn*, Illinois, USA.

Basone, F., Cavaleri, L., Di Trapani, F., Muscolino, G., 2017, Incremental dynamic based fragility assessment of reinforced concrete structures: Stationary vs. non-stationary artificial ground motions, *Bull. Earthquake Eng*, **103**,105-117.

Castaldo, P., Gino, D., Bertagnoli, G. Mancini, G., 2020. Resistance model uncertainty in non-linear finite element analyses of cyclically loaded reinforced concrete systems, *Eng Struct,* **211**, 110496.

Castaldo, P., Gino, D., Mancini, G., 2019. Safety formats for non-linear analysis of reinforced concrete structures: discussion, comparison and proposals, *Eng Struct*, **193**, 136-153.

Cavaleri, L., Zizzo, M., Asteris, P.G., 2019. Residual out-of-plane capacity of infills damaged by in-plane cyclic loads, *Eng Struct*, **209**, 109957.

De Risi, M.T., Di Domenico, M., Ricci, P., Verderame, G.M., Manfredi, G., 2019. Experimental investigation on the influence of the aspect ratio on the in-plane/out-of-plane interaction for masonry infills in RC frames, *Eng Struct*, **189**, 523–540.

Di Trapani, F., Malavisi, M., 2019. Seismic fragility assessment of infilled frames subject to mainshock/aftershock sequences using a double incremental dynamic analysis approach, *Bull. Earthquake Eng*, **17**(1), 211–235.

Di Trapani, F., Giordano, L., Mancini, G., 2020a, Progressive Collapse Response of Reinforced Concrete Frame Structures with Masonry Infills, *J. Eng. Mech.,* **146**(3), 04020002.

Di Trapani, F., Bolis, V., Basone, F., Preti, M., 2020b, Seismic reliability and loss assessment of RC frame structures with traditional and innovative masonry infills, *Eng Struct*, **208**, 110-306.

Di Trapani, F, Shing, P.B., Cavaleri, L., 2018a. Macroelement model for in-plane and out-of-plane responses of masonry infills in frame structures, *J Struct Eng,* **144**:04017198.

Di Trapani, F., Bertagnoli, G., Ferrotto, M.F., Gino, D., 2018b. Empirical equations for the direct definition of stress-strain laws for fiber-section based macro-modeling of infilled frames, *J Eng Mech*, **144**(11), 04018101.

Eurocode 6. Design of Masonry Structures. Part 1-1: General Rules for Reinforced and Unreinforced Masonry Structures. Brussels, 2005.

Furtado, A., Rodrigues, H., Arêde, A., Varum, H., 2015. Simplifed macro-model for infll masonry walls considering the out-of-plane behaviour, *Earthq Eng Struct Dyn* **45**(4), 507-524.

Furtado, A., Rodrigues, H., Arêde, A., Varum, H., 2016. Experimental evaluation of out-of-plane capacity of masonry infill walls, *Eng Struct,* **111**, 48–63

Longo, F., Wiebe, L., da Porto, F., Modena, C., 2018. Application of an in plane/out of plane interaction model for URM infill walls to dynamic seismic analysis of RC frame buildings, *Bull Earthquake Eng*, **16**, 6163-6190.

Mazza, F., 2019. In-plane–out-of-plane non-linear model of masonry infills in the seismic analysis of r.c.-framed buildings, *Earthq Eng Struct Dyn* **48**(4), 432-453.

McKenna, F., Fenves, G.L., Scott, M.H., 2000. Open system for earthquake engineering simulation. University of California, Berkeley.

Mosalam, K.M., Günay, S., 2015. Progressive collapse analysis of RC frames with URM infill walls considering in-plane/out-of-plane interaction, *Earthq Spectra,* **31**(2), 921-943.

Ricci, P., Di Domenico, M., Verderame, G.M., 2018. Experimental assessment of the in-plane/out-of-plane interaction in unreinforced masonry infill walls, *Eng Struct,* **173**, 960–978

Ricci, P., Di Domenico, M., Verderame, G.M., 2019. Out-of-plane seismic safety assessment of URM infills accounting for the in-plane/out-of-plane interaction in a nonlinear static framework, *Eng Struct* **195**, 96–112.

Vamvatsikos, D., Cornell, A.C., 2002. Incremental dynamic analysis. *Earthq Eng Struct Dyn*, **31(3)**, 491–514.